Evolution of Yohkoh Observed White Light Flares

Barbara Sylwester and Janusz Sylwester
Space Research Centre, Polish Academy of Sciences, PL 51-622 Wroclaw, Kopernika 11, (e-mail: bs,js@cbk.pan.wroc.pl)

October 7, 1999

Abstract. We consider in detail the evolutionary patterns of few white light flares observed by *Yohkoh.* The following data have been used in the analysis: sequences of deconvolved SXT images in X-ray and optical filters, MEM–reconstructed HXT images and the other supporting data. The resolution in the deconvolved images is below 1 arc sec. Working with sequences of deconvolved images makes it also possible to investigate the *dynamics* of these structures with high spatial accuracy. Comparison of the morphology of flare brightenings as observed in hard, soft and optical ranges reveals that these emissions are not co-spatial and are most probably related to different plasma volumes at any instant. These observations cannot be easily accommodated within standard flare scenarios. Traditionally, the hard and optical flare emissions are expected to be co-spatial and the soft X-ray emission is presumed to fill the coronal portion of flaring loop(s) during rise phase. Present observations do not easily fit to such scenario.

Keywords: Sun, flares, white-light

1. Introduction

We have investigated five flares recorded by the instruments aboard the *Yohkoh* satellite during its early period of operation when the aspect sensor images have been available. The analysed events belong to the white-light (WL) flare class. The routine measurements of the flare optical emission have been made using the aspect sensor with the filter centered at 4308 Å. The width of the spectral filter used is $\sim$ 30 Å (the CN band). The aspect sensor images represent the first observations of WL flare emission as obtained without seeing effects (since they have been made from outside the Earth's atmosphere). *Yohkoh* has observed several WL flares and a number of papers have been devoted to their analysis (Hudson *et al.*, 1992, Hudson, van Driel-Gesztelyi and Kosugi, 1994, Matthews, Brown and van Driel-Gesztelyi, 1996). The earlier ground-based WL observations revealed an unusual behaviour of K1 in the Ca II K line for the flare on 11 October 1974 as reported by Fang *et al.* The time series of Balmer line profiles have been analysed by Lee *et al.*, (1996) for the flare on 27 October 1991. In particular they have observed the asymmetry of low Balmer emission line profiles using the multi-channel spectrograph attached to the Solar Tower Telescope of Najing University. This asymmetry has been analysed in order to

Table I. The main characteristics of the investigated flares.

No.	Date	UT	Hα	*GOES*	Location	NOAA	I_{max}/I_0	Correl.
1	24 Oct. 1991	22:40	1N	M9.8	S12 E46	6891	1.06	*GOES*
2	15 Nov. 1991	22:38	3B	X1.5	S13 W19	6919	1.35	L
3	03 Dec. 1991	16:38	2B	X2.2	N17 E72	6952	1.05	M1
4	26 Jan. 1992	15:31	3B	X1.0	S16 W66	7012	1.10	L
5	24 Apr. 1992	19:19	2B	M1.2	N13 W00	7138	1.05	L

derive the information on the dynamics of the hydrogen cloud in the flare region. This particular flare has been also observed by *Yohkoh* but no inter-comparison has been made between the results. The excitation mechanisms of WL flare emission are still not known although the theoretical considerations have been presented in the literature quite often (Rieger *et al.*, 1996, Ding, Fang and Yun, 1999). However it is commonly accepted that the origin of optical continuum of WL flares should be associated with accelerated particle beams penetrating denser regions. This concept is based mainly on the investigations of temporal correlation (generally good) between WL flare emission and accompanying hard X–ray and microwave emissions. It is believed that beams of energetic electrons and/or protons bombard the lower solar atmosphere thus contributing to flare continuum emission.

The spatial relation of optical and hard X-ray emissions became possible to be investigated accurately only after the *Yohkoh* launch. Matthews, Brown and van Driel-Gesztelyi (1998) compared the locations of white light patches and hard X-ray sources for four WL flares observed by *Yohkoh*. They have used the original aspect sensor images as obtained in full resolution (pixel size 2.45×2.45 arc sec) and the reconstructed Hard X-ray Telescope (HXT) images as seen in 33 - 53 keV (M2 channel).

The *Yohkoh* data provide the opportunity to study the flare images in the wavelength interval from optical (NaBan filter), through soft X–ray emission (SXT images) to hard X–rays (HXT data). By using the advanced methods of image processing it is possible to increase the spatial resolution and the accuracy of image co-alignment.

2. Observations and Data Processing

From among 10 flares for which the observations of flare related WL emission have been reported, we have selected for detailed analysis

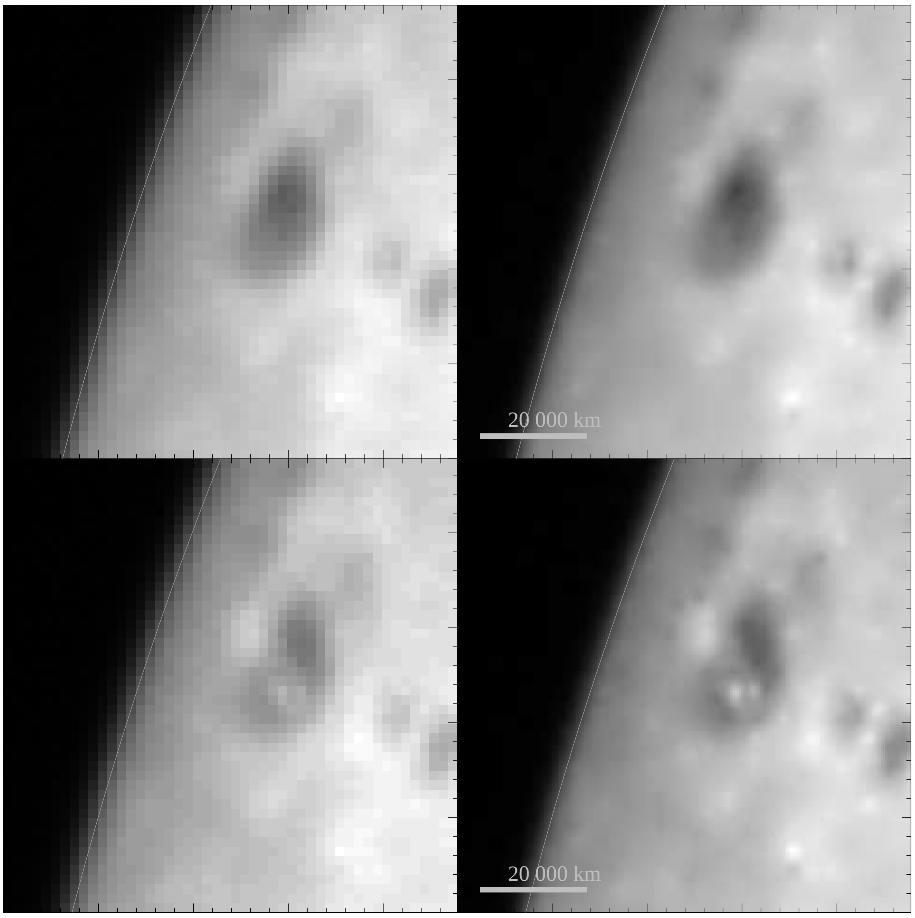

Figure 1. The original (left panel) and deconvolved (right) optical images (NaBan filter) for the flare on 3 December 1991. In the upper row initial flaring image taken at 16:33:37 UT (the first available) is shown while in the lower row the image taken at the WL flare maximum (16:36:39 UT) is displayed.

the five strongest events. Main characteristics of the flares selected are presented in Table I. The data set used in the present analysis consists of flare sequences of the Soft X-ray Telescope (SXT) and aspect sensor images taken in full resolution. These images (64×64 pixels) have been deconvolved using ANDRIL algorithm (Sylwester and Sylwester, 1998). The deconvolution removed the image blurring due to the instrument point spread function and increased numerically the spatial resolution in the images down to 1 arc sec. As a result of deconvolution we obtained corresponding sequences of images (320×320 sub-pixels; with 5×5 sub-sampling). It is known, that oversampling (super-resolution techniques) do introduce additional uncertainty towards the restored intensity images due to ill-conditioned nature of the problem. This has been studied in details for case of ANDRIL SXT image deconvolution algorithm by Sylwester and Sylwester, (1999). Using the results of this study it is possible to assign uncertainty to each of intensity values as obtained in the process of deconvolution. A typical uncertainty increase has been found to be around a factor $4 \div 5$. In areas of high signal-to-noise values (white light images, maxima of X-ray emission) this increase of uncertainty does not noticeably influence the results of the present study. The deconvolved images have been carefully co-aligned to within the fraction of arc sec as discussed further-on.

2.1. The Flare on 3 December 1991

As the first example we present the analysis of the most intense *GOES* flare from our set of analysed flares. This was X2.2 flare which occurred close to the solar limb (N17 E72) at 16:38 UT. The value of flare WL emission contrast (brightness relative to pre-flare level) is 1.05 as can be seen in the last column of Table I.

In Figure 1 we present the examples illustrating how the deconvolution improves the original NaBan images. The left panel presents the central portion (48×48 SXT pixels) of the original image. In the upper row the initial flare image is shown while in the lower row the image recorded during the WL maximum phase is displayed for the comparison. The limb position is indicated by thin line. The right panel shows the corresponding deconvolved images (240×240 sub-pixels). On the deconvolved images more details can be recognized in comparison with the original images. These details can be better resolved in the positive fixed differences image shown in Figure 2. (The fixed differences images are obtained by subtracting the first deconvolved pre-flare image from the whole sequence.) Two patches (southern and northern) can be easily distinguished. The southern patch consists actually of two separate point-like sources at this phase of the flare evolution. This southern pair of sources can also be distinguished in the frame taken 8 s earlier (as shown in Figure 4). The distance between individual sources within a pair is about 3000 km only. The fainter, more extended patch of WL emission is seen to the North of this southern patch. One may notice that perfect coalignement of the images within a sequence has been obtained since in the fixed differences images the solar limb is virtually indistinguishable. Even a slightest (greater than 1/10 arc sec) misalignment, would result in a substantial signal on a difference image for regions of high contrast, like solar limb or sunspots. This perfect co-alignment we have achieved by using dedicated image correlation algorithm based on the idea of additional pointing correc-

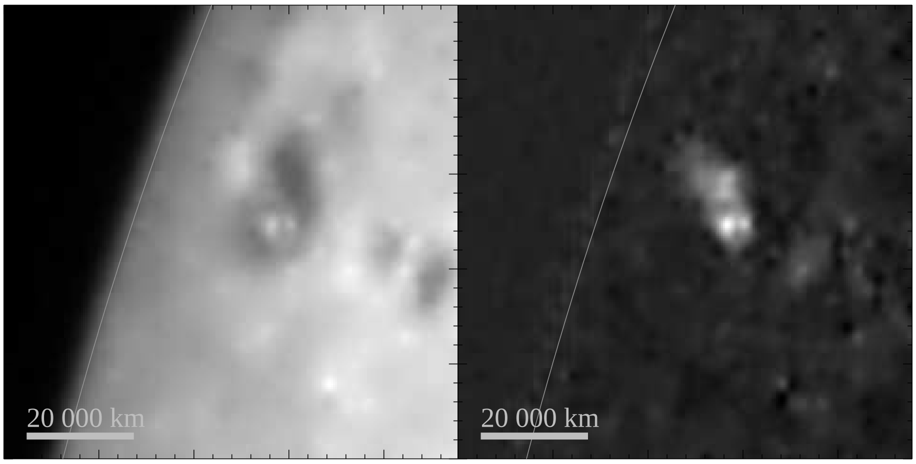

Figure 2. The WL deconvolved (left) and fixed differences (relative to initial frame) image for the maximum phase (16:36:39 UT) of 3 December 1991 flare. See text for details.

tions discussed by Siarkowski et al. (1996). In case of deconvolved optical images we allowed for the additional (fractions of sub-pixel) alignment shifts in order to reach the best image correlation between reference (initial) and analysed frames. The *negatives* of WL images have been used in cross-correlation. By doing this we avoid problems due to the white-light contribution of the flare itself. As the parameter being optimized in the correlations, we have used the following "surface distance" characteristic q:

$$q = \frac{\sum_{\rm i} (I_0 - I_{\rm k})^2}{n_{\rm i}} \ , \tag{1}$$

where I_0 is the normalized (integral intensity) reference image, $I_{\rm k}$ is a normalized image to be shifted (k$^{\rm th}$ frame) and $n_{\rm i}$ is the number of elements (sub-pixels) in the given image. In order to follow the time changes of analysed flare emissions we present in Figure 3 the light curves (*GOES*, NaBan and HXT M2 channel) for the first 10 min of initial flare evolution. The dashed vertical lines point to the times for which the white light emission contours are displayed in Figure 4. It is seen that during the very beginning of the event (around 16:35 UT), the WL emission (integrated over entire flaring area) slightly precedes the hard X-ray emission. During the impulsive rise phase both emissions are nearly synchronous. After the maximum phase, the hard X-ray emission (M2 channel) decays much faster although individual common spikes can still be identified on both curves. In Figure 4 the contours of WL fixed differences emission are presented for selected times covering the period of about 7 min. The thick line connects two main patches

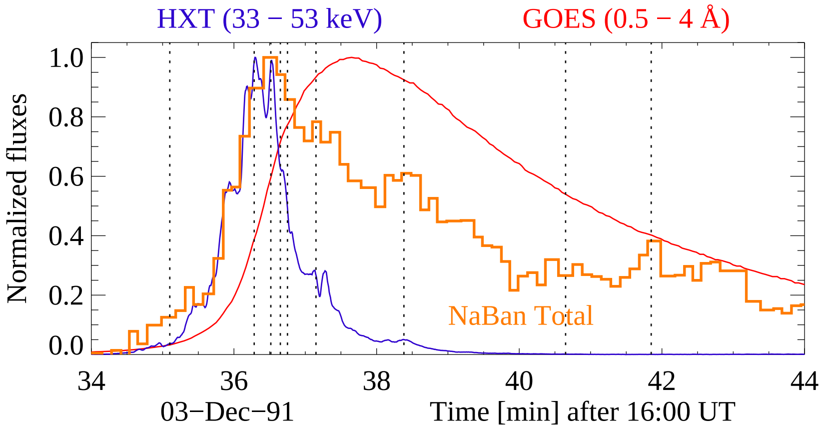

Figure 3. The hard X-ray (M2 HXT), optical (NaBan) and soft X-ray (*GOES* 0.5–4 Å) fluxes for 3 December 1991 flare. The dashed vertical lines indicate nine times at which the contours are presented in the next Figure.

(northern and southern) which preserve their identity during the investigated period. Fast, systematic changes of the morphology of WL emission can be recognized. During the early flare phase the northern patch dominates. Around flare maximum two patches coexist with the southern one becoming more intense and structured (double, as shown in Figure 2). The relative importance of northern and southern patches is similar during the early decay. Later on an additional compact, well separated region develops in the south-western part of the investigated area. Although it does not dominate the total WL flare emission, it is significant for about 4 min during late decay phase. On the right bottom frame in Figure 4 we have indicated three selected areas called **a**, **b** and **c**. In the upper panel of Figure 5 the time variations of NaBan fluxes integrated within the selected sub-areas are presented. In order to allow for better visualization, the base levels of the vertical scale for curves **a** and **b** are displaced vertically as indicated by dashed horizontal lines at the onset of each plot. In the lower panel of Figure 5 the hard X-ray light-curves are presented. In this case individual light-curves have also been shifted vertically. It is seen that the emission in all sub-areas chosen rise nearly simultaneously with the emission in M2 HXT channel. The onset of WL emission is slightly delayed for region **c**. The rise time profile for all three regions is nearly the same and amounts to $\sim$ 1 min. The most dynamic and intense in WL is the emission in the area **a**. The full width at half maximum (FWHM) of NaBan light curve for this area is $\sim$ 2 min only. The emission in the faintest area (**c**) has similar behaviour in this respect. However for

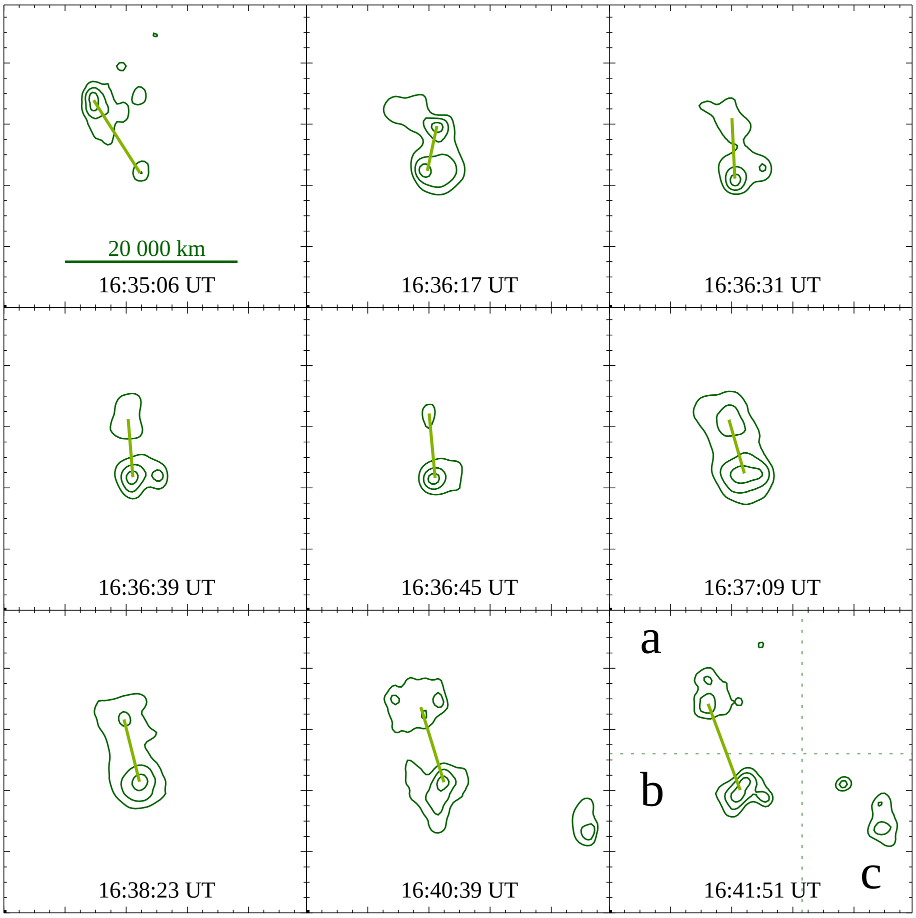

Figure 4. The sequence of optical (NaBan filter) deconvolved fixed differences image contours for 3 December 1991 flare. Contours are plotted at levels 0.5, 0.7 and 0.9 of the maximum for individual frames. The frames presented correspond to times indicated in Figure 3. Thick gray line connects the centres of gravity for the main patches and its length indicates the distance. Note the change of inclination of this interconnecting line. The dashed lines on the last image divide the 100×100 sub-pixels area into three sub-regions (**a**, **b** and **c**).

area **b**, the FWHM of WL curve amounts to $\sim$ 4 min. This region persists for much longer time in comparison with regions in areas **a** and **c**. It decays much slower following rather the soft X–ray (*GOES* light curve) with a kind of plateau seen after the maximum. In this context it seems interesting to investigate the possible correlations of the emissions variability in various energy bands for individual areas. In Figure 6 we present correlation diagrams in which the dependence between the WL emission (NaBan filter), soft X-ray radiation (*GOES* $0.5 - 4\,\text{Å}$) and hard X-ray radiation (all HXT channels) are displayed

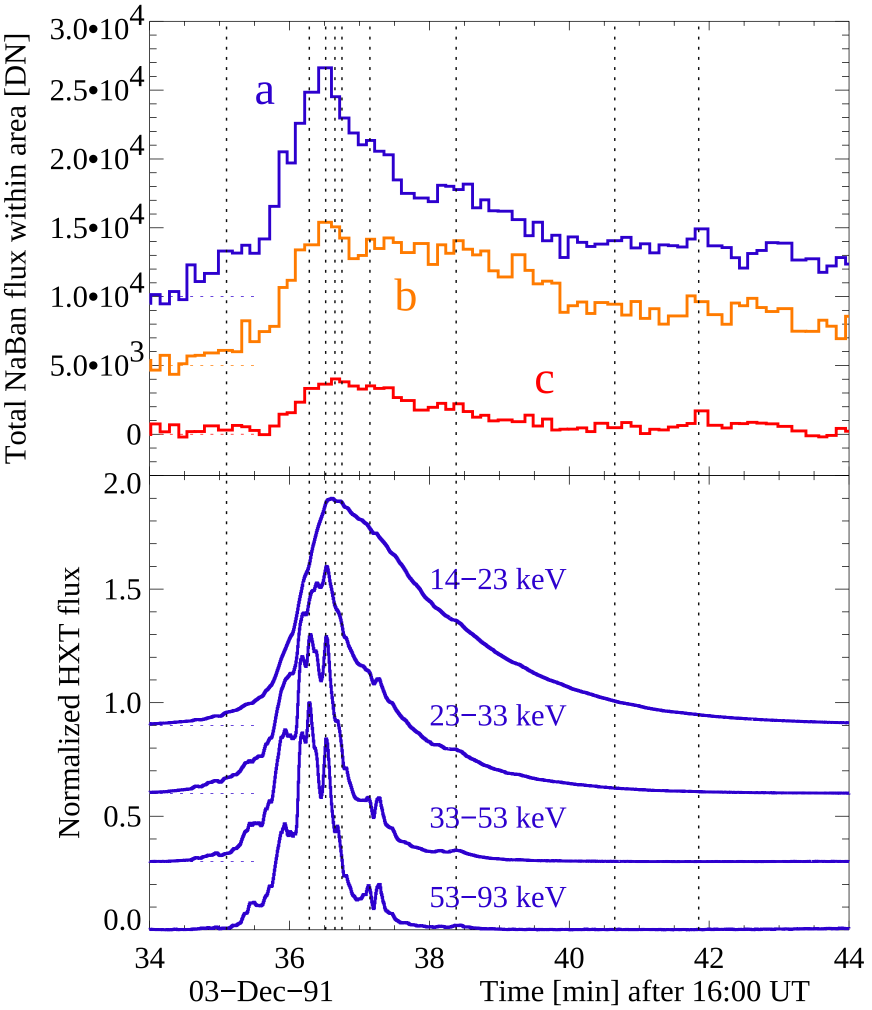

Figure 5. The upper panel shows the optical light curves (NaBan filter) for three areas (**a**, **b**, **c**) of 3 December 1991 flare. The location of the areas is indicated in Figure 4. In the lower panel the flare-integrated hard X-ray light-curves are shown for all channels of HXT. The curves are vertically displaced for the sake of better visualization. Corresponding base levels are indicated as dashed horizontal lines at the onset of each plot.

for regions **a**, **b** and **c** separately. The plots have been normalized. The colour (shades) of data points and the connecting lines are time dependent as indicated by colour bar at the top of the Figure. Darker points represent earlier times. Generally it is difficult to find one-to-one correlation between WL and specific X-ray radiation during entire investigated period. The best correlation is observed between the WL and M1 HXT channel (23-33 keV) emissions for the area **a**. In order

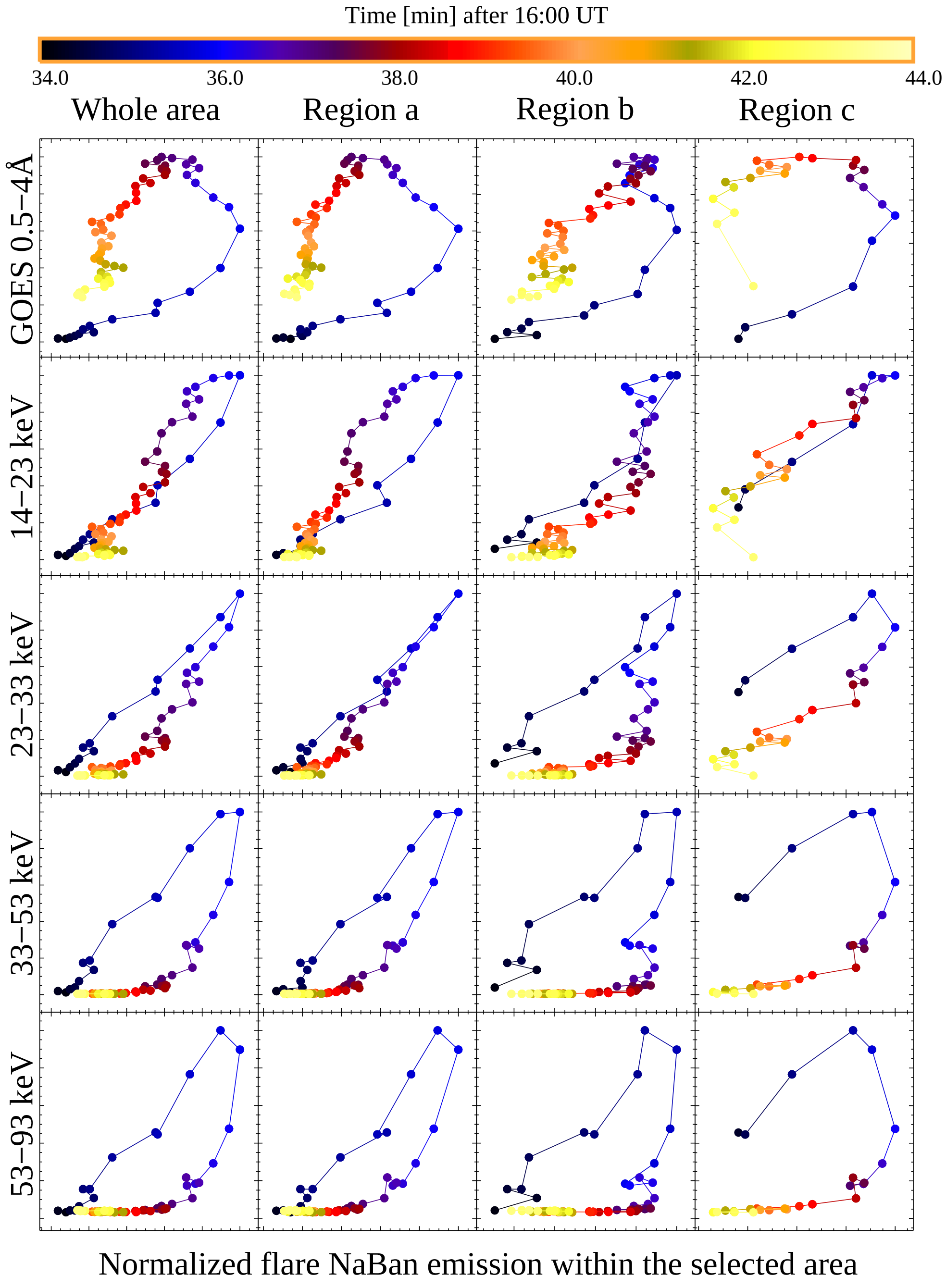

Figure 6. The diagrams of the WL (NaBan filter) vs X-ray radiation for the entire flare FOV and for individual selected regions (**a**, **b**, **c**) of 3 December 1991 flare. The X-ray flux represents the total flare emission in each case. See the text for details.

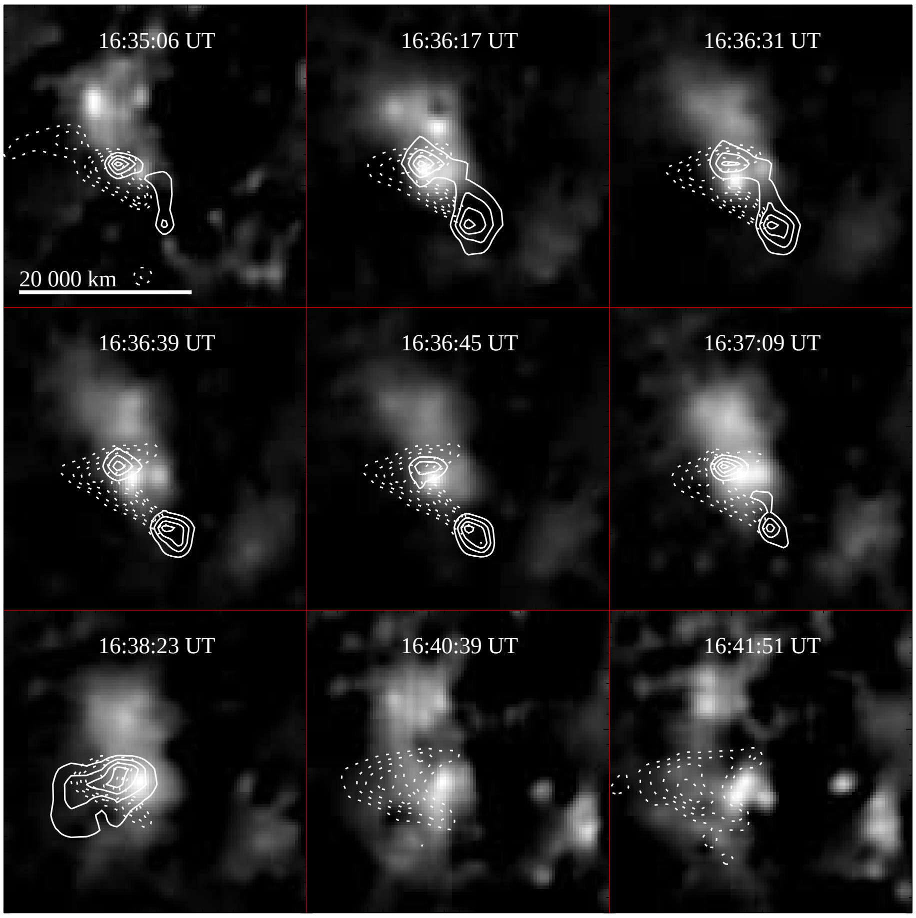

Figure 7. The sequence of WL (NaBan; gray scale), SXT (Al12; dashed contours) and HXT (M2; solid contours) are superposed for 3 December 1991 flare. For the last two frame the M2 signal was too weak to allow for HXT image reconstruction. See text for details.

to better understand the observed relation of the WL and X-ray emissions of the flare, we attempted to compare the spatial location of the sources contributing to investigated emission bands. In Figure 7 the sequence of nine images for times indicated by vertical dashed lines in Figure 3 are presented. The 49×49 arc sec field of view containing the main flaring structures has been selected. In the background, the NaBan fixed positive differences image is displayed in the grey scale. The dashed line contours over-plotted represent the emission in the SXT Al12 deconvolved images while the MEM reconstructed hard X-ray images (M2 HXT channel) are shown as superimposed solid line contours. The contours are drawn at the levels: 0.3, 0.5, 0.7 and 0.9 of respective maximum values for individual frames. The frames selected cover the entire WL flare phase and represent characteristic times of flare evolution, mostly when individual spikes are observed on the hard X-ray light-curve (see Figure 3). It is evident from the images presented in Figure 7 that the morphology of WL and X-ray emission is different and changing fast during the evolution. The most dynamic changes take place during the rise and decay phases while during the maximum phase the morphology of X-ray radiation does not change substantially. The soft X-ray emission is rather elongated at the onset of the impulsive phase and becomes crescent-shaped later on. The hard X-ray emission (M2 HXT) is rather compact at the beginning and is concentrated in two small patches located $\sim$ 9000 km South to the brightest optical emission. At this phase the WL emission centres are not at all co-spatial with the X-rays. One of M2 patches is elongated in N-S direction and the second, more intense is round in shape. Later on during the flare WL maximum phase, both patches are round and well separated. During the WL decay the northern patch ceases the first.

It is clearly seen that the optical, soft and hard X-rays are not co-spatial (according to our best co-alignment). Only the northern patch seen at 16:36:17 UT frame appears to be co-spatial for all emissions displayed (optical, Al12 SXT and M2 HXT). However this represents the one and only perfect co-alignment case and therefore could be regarded as a coincidence (result of projection effect).

From inspection of Figure 7 it is also seen that substantial changes took place in the morphology of various emissions during the investigated period (few minutes of initial flare evolution). The WL emission is concentrated North to the X-ray emission in the initial frame while in the last frame presented, the WL emission is concentrated in the central part of the frame apart the maxima of soft and hard X-ray emission patches.

In order to better compare the location of emission in various energy bands we present in Figure 8 the MEM reconstructed HXT images for all four channels at the time of hard X-ray flare maximum (16:36:39 UT) together with Al12 and WL emission contours superimposed. It is seen that at this particular time the best spatial overlapping between the WL and X-ray sources is observed for lower energy HXT channels (L and the M1) while the largest displacement is observed for the highest energy range (53-93 keV; H channel). The strongest patch of M1 channel emission is almost co-spatial with that observed in soft and optical bands. For the HXT H channel the maxima of optical and hard X-ray emissions are separated by $\sim$ 9000 km in projection.

Based on inspection of Figures 4 and 7 it is evident that during almost all investigated period two patches of emission can be distin-

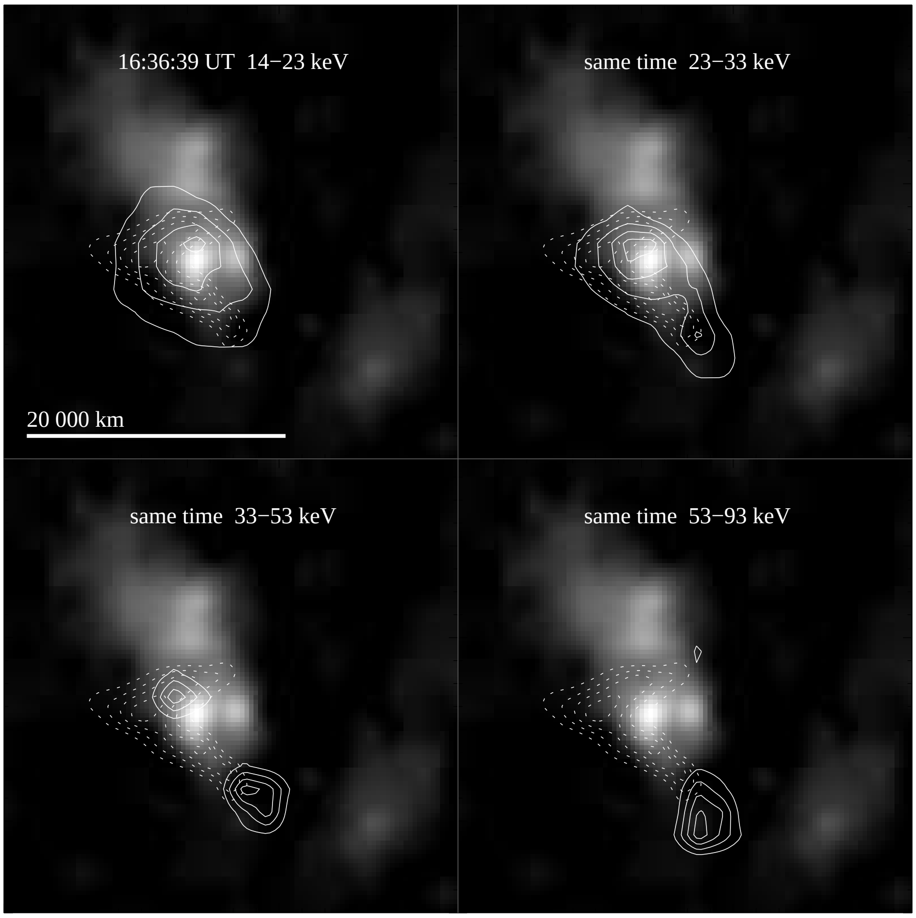

Figure 8. The WL (NaBan) deconvolved image for the flare of 3 December 1991 at 16:36:45 UT (grey scale) superposed with the contours of MEM reconstructed HXT images for all four channels (the solid line). Also shown are SXT (Al12) deconvolved images (dashed lines) taken at closest available times (few seconds apart). The contours are drawn at the levels of 0.3, 0.5, 0.7 and 0.9 of the respective maximum values.

guished both in the WL and in hard X-ray range. The time variations of the distance between these two patches are plotted in the middle panel in Figure 9. At the beginning of flare the distance between these two patches decreases quickly for 1 min as observed in WL and HXT emissions. Afterwards a slow increase of the distance between two patches can be noticed. The displacement amounts to $\sim$ 10 arc sec during 8 minutes of evolution. Similar trend can also be observed for the evolution of the M2 HXT patches. However only about 2 min of evolution can be followed in this case. The dominant emission patches behave differently in hard X-ray and WL ranges. The hard X-ray patches are

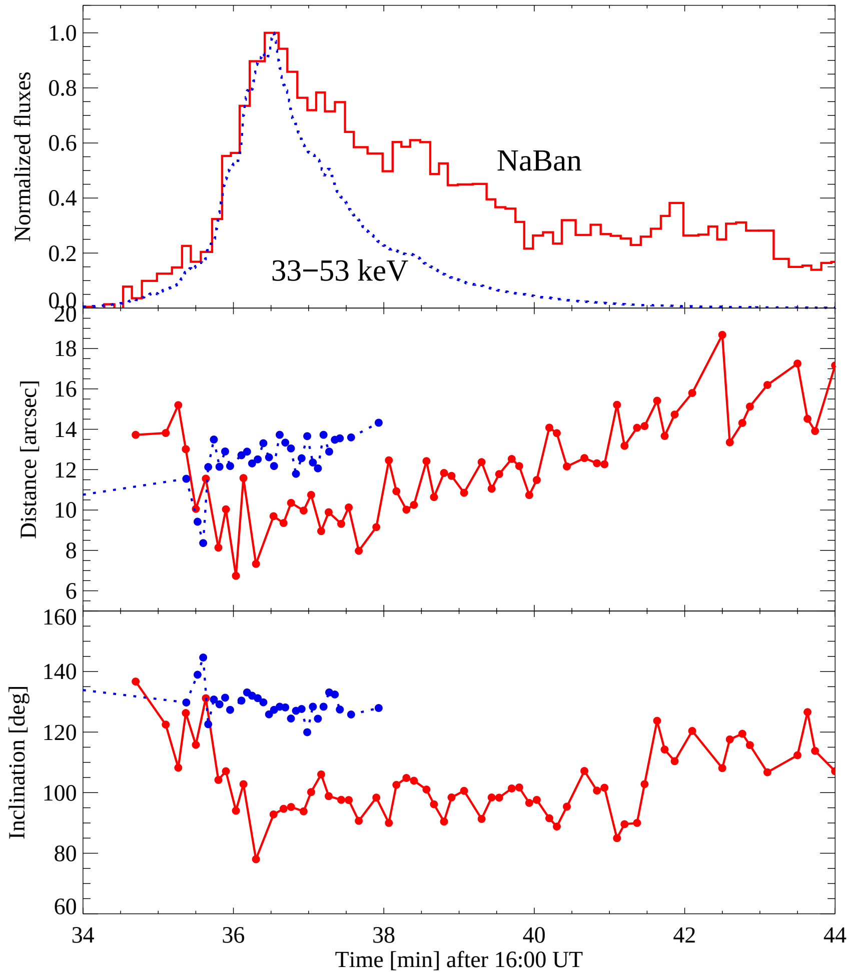

Figure 9. The time variations of the distance (the middle panel) and inclination (bottom panel) between two main patches observed on NaBan deconvolved images (solid line) and M2 HXT images (dotted line) for the flare on 3 December 1991. The top panel shows corresponding NaBan and M2 HXT normalized light curves for the comparison.

more separated except for the very beginning of the rise phase. In the bottom panel of Figure 9 we present the time variations of inclination of the line connecting the two patches. After the initial drop of this angle (flare rise) inclination does not change substantially fluctuating around the average value of about 95° for about 5 min. Later on this inclination assumes another average value ($\sim 115°$) for the last 2 min of observations. The average inclination of the line connecting the hard

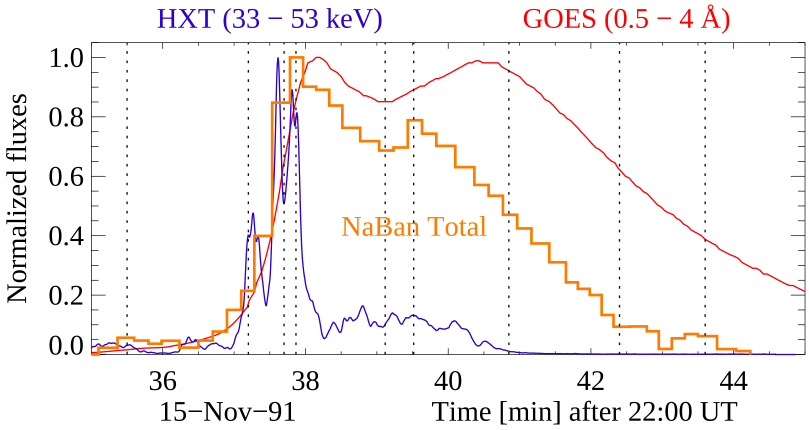

Figure 10. The hard X-ray (M2 HXT channel), optical (NaBan) and soft X-ray (*GOES* 0.5–4 Å) light curves for 15 November 1991 flare. The dashed vertical lines indicate the times at which the images in Figure 11 are presented.

X-ray patches corresponds to different value $\sim 135°$ after the initial excursion.

2.2. The Flare on 15 November 1991

The second flare we would like to present is the brightest event in Hα (3B) from our set. The flare occurred on the disc (S13 W19) at 22:38 UT and has already been well-studied (more than 15 related papers have been published). It is the flare with the highest WL contrast (1.35; see Table I) among the set of events considered. Hudson *et al.*, (1992) reported the contrast value of 1.38 for this event. Below we display the sequence of Figures presenting the results of analysis for this flare. The results are shown in a way similar to that adopted in case of 3$^{\mathrm{rd}}$ December 1991 event. In Figure 10 the light curves for selected energy ranges (*GOES*, NaBan and M2 HXT) are presented. The nine vertical dashed lines indicate the times for which the locations of WL sources are displayed in Figure 11.

The dynamic behaviour of the WL flare morphology is evident from the inspection of Figure 11. The first frame shown corresponds to the pre-flare phase (22:35:42 UT). Two main patches (in areas **a** and **b**) change their relative position (move away and turn around) during the entire evolution. The fainter patch (in area **c**) does not change its position. The NaBan light curves for these individual patches are presented in the upper panel of Figure 12. A double component light curves are seen for all selected areas. The first component corresponds in time to a hard X-ray impulsive burst while the second is connected

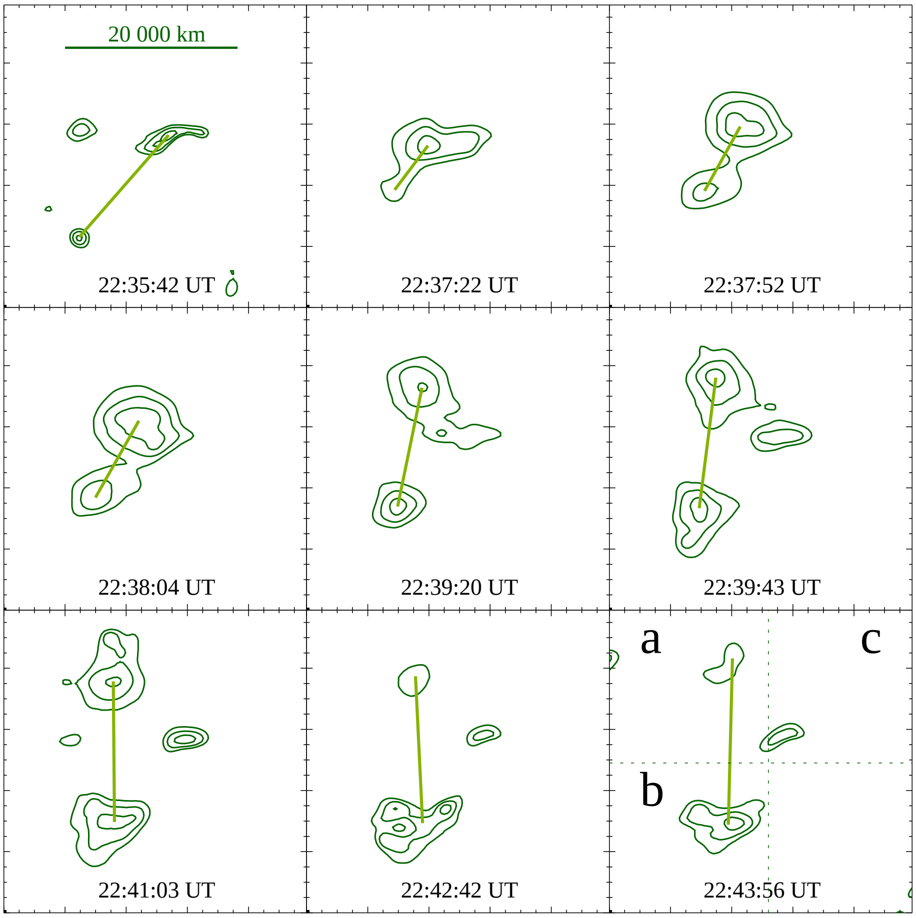

Figure 11. The sequence of WL (NaBan) deconvolved fixed differences images of 15 November 1991 flare made at selected times during the flare (as indicated by the vertical lines in Figure 10). The contours are drawn at the levels 0.5, 0.7 and 0.9 of respective maximum values. The dashed lines on the last image divide the 100×100 sub-pixels area into three sub-areas (**a**, **b**, **c**) containing the patches being analysed. The thick gray line connects the emission centres of the characteristic patches and its length defines the distance between them.

with the gradual part of this flare. The WL emission coming from the southern area (**b**) is of nearly the same intensity for the first and second component. The correlation diagrams between the WL and the other types of integrated flare emission are presented in Figure 13. Again the colour (shade) of data points is related with the time elapsed from the start of the event. The darkest points represent the initial phase. In case of the 15 November 1991 flare, the best correlation can be observed between the optical and HXT L channel (14-23 keV) emissions except for sub-area **c**. The relative locations of WL, soft and hard

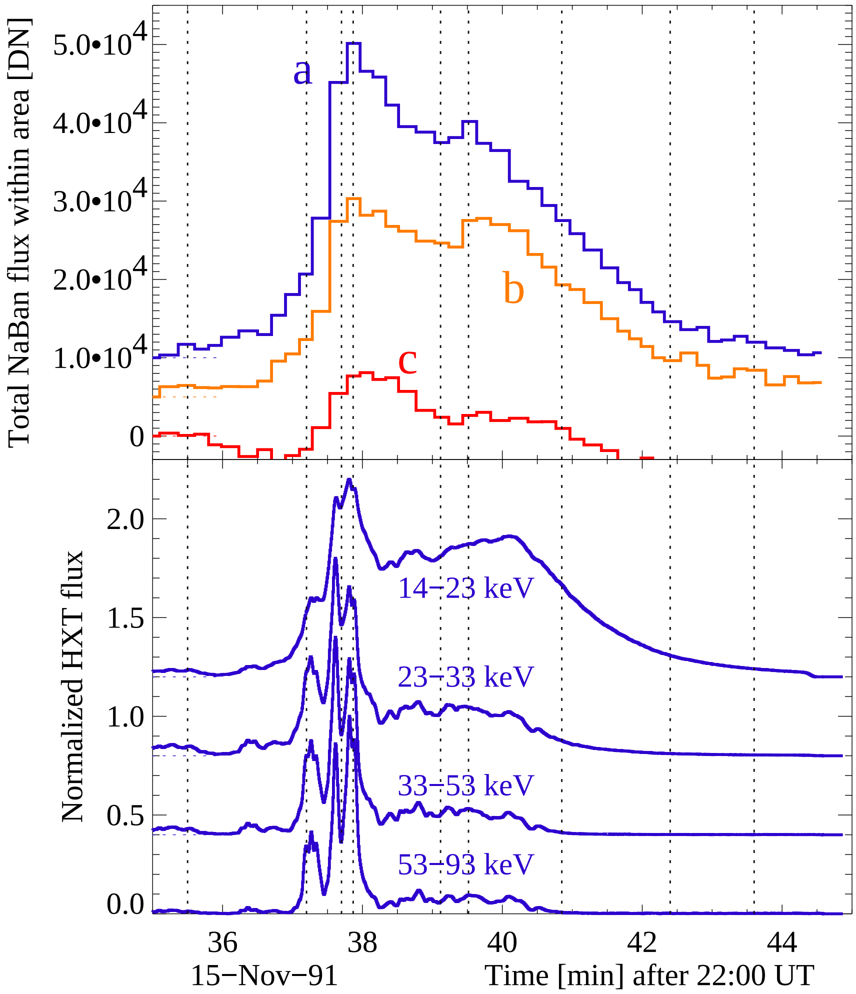

Figure 12. The upper panel shows the WL light curves (NaBan filter) for three sub-areas (**a**, **b**, **c**) of 15 November 1991 flare (as indicated in Figure 11). The lower panel shows the light curves of integrated hard X-ray flux as measured in all channels of HXT. The curves are vertically displaced for the sake of better visualization. Corresponding zero levels are indicated as dashed horizontal lines at the onset of each plot.

X-ray emissions (grey scale, dashed and solid contours respectively) during 15 November 1991 flare are presented in Figure 14 for selected times. The size of individual frame is (49×49 arc sec). On the last two frames (the late decay phase) the hard X-ray emission is too faint for the image to be reconstructed. The location of NaBan, Al12 and HXT M2 emission centres do not coincide during the flare. The closest are Al12 and M2 emissions in the second frame (22:37:12 UT) corre-

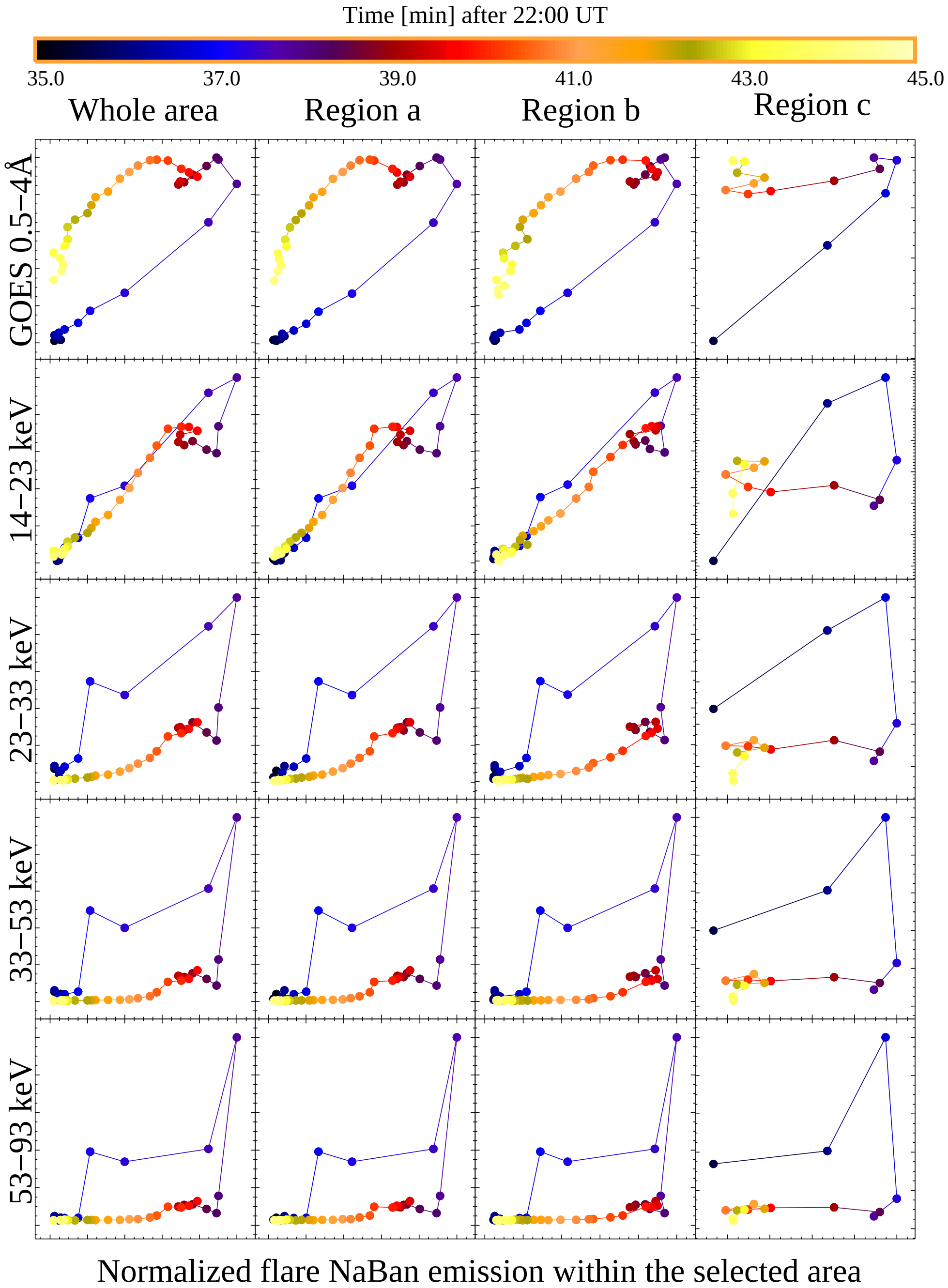

Figure 13. The diagrams of the WL (NaBan filter) vs X-ray radiation for three sub-areas (**a**, **b**, **c**) of 15 November 1991 flare.

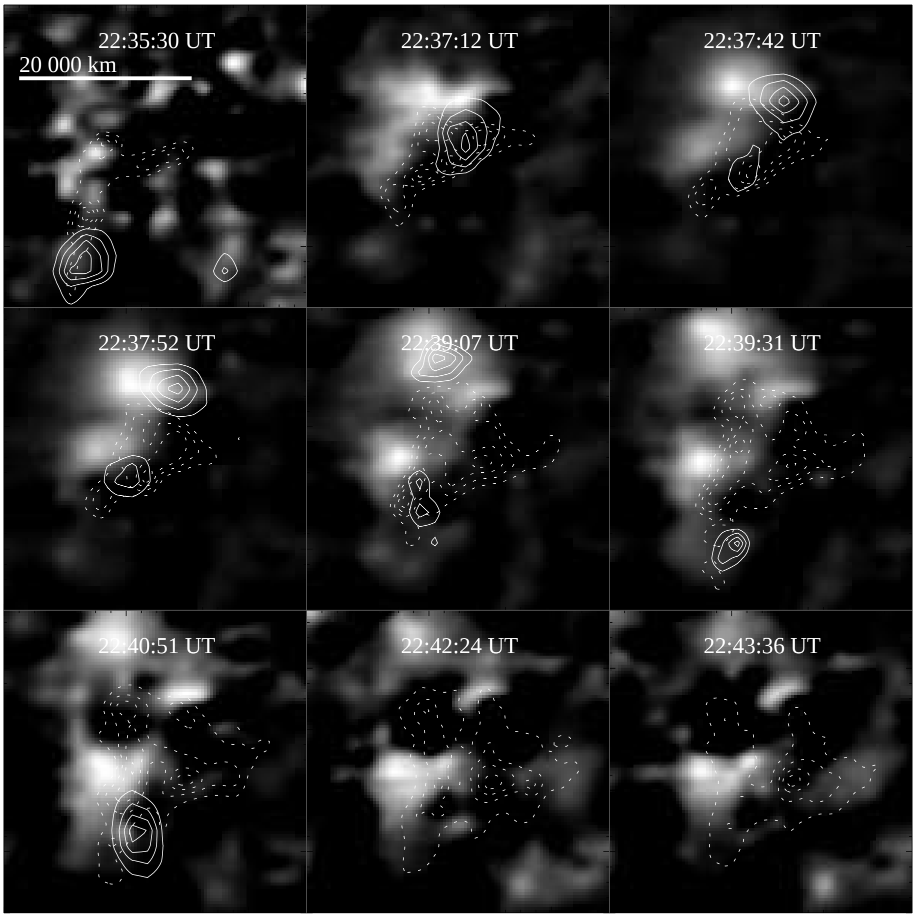

Figure 14. The sequence of NaBan, Al12 SXT and M2 HXT superposed images for nine selected times (cf. Figure 10) of 15 November 1991 flare.

sponding to the first hard X-ray spike on the light curve. However this overlapping does not hold for the other times. The WL emission is displaced in comparison with X-rays for all frames analysed. This can be best seen on sequences of animated images available at `www.cbk.pan.wroc.pl/publications/1999/white_light.htm` for this and the other flares from Table I. We welcome the reader to visit this web place. There are also available the colour versions of all the Figures from the present study.

The overall relative location of WL, soft and hard X-ray emissions for the time of flare maximum (22:37:52 UT) is shown in Figure 15. At this time the location of maximum HXT L channel emission (14-23 keV) is nearly co-spatial (to within 2 arc sec in projection) with the soft X-ray emission maximum (Al12). In the higher energy bands

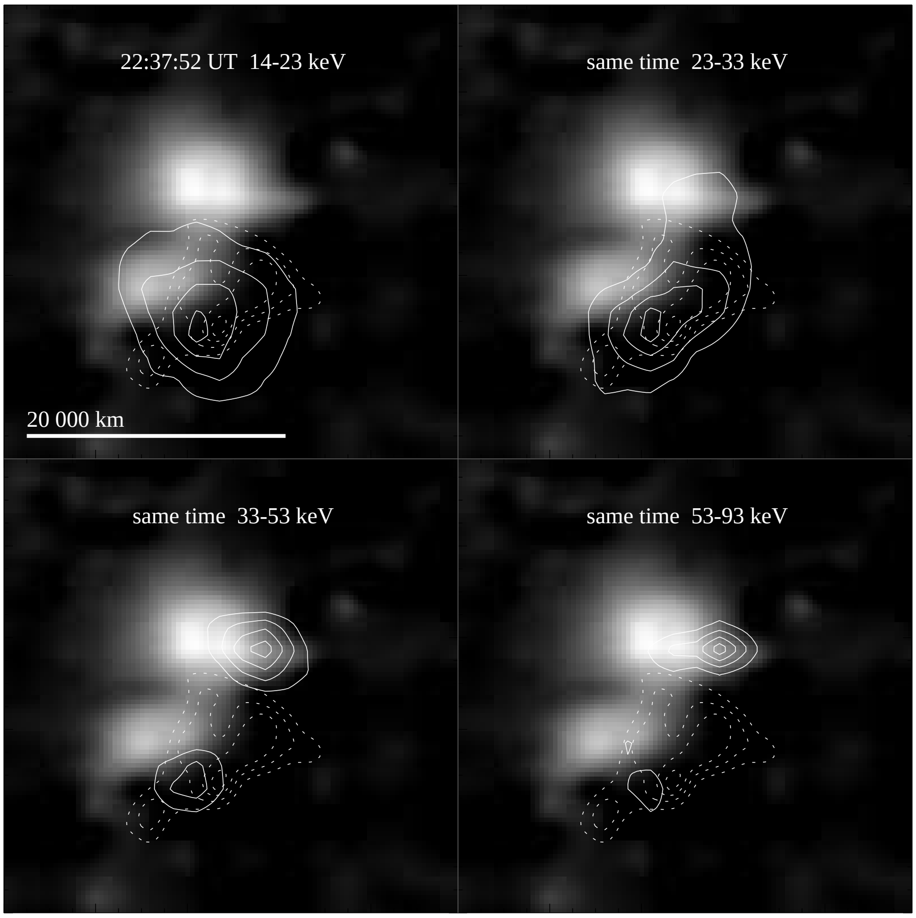

Figure 15. The NaBan fixed differences positive image for the flare of 15 November 1991 at 22:37:52 UT (in background, grey scale) superposed with the contours of MEM reconstructed HXT images for the four channels of HXT (solid lines) and SXT Al12 (dashed lines) deconvolved images at the closest available times. The contours are drawn at 0.3, 0.5, 0.7 and 0.9 of respective maximum values.

of HXT (M2 and H channels) the two characteristic emission patches are seen both in WL emission and X-rays. They are not at the same location however. The respective emission centres for WL and HXT are displaced by $\sim$ 6000 km. We believe that the relative coalignment we have made is to within 1 arc sec when images of the same band are considered. We also believe that the observed displacements between hard X-ray and WL emission are real since it is not easy to bring the overall picture into perfect match by applying a simple shift of the boresight for individual spectral bands. Even by forcing perfect match for a particular time and spectral band, we fail to observe this match to

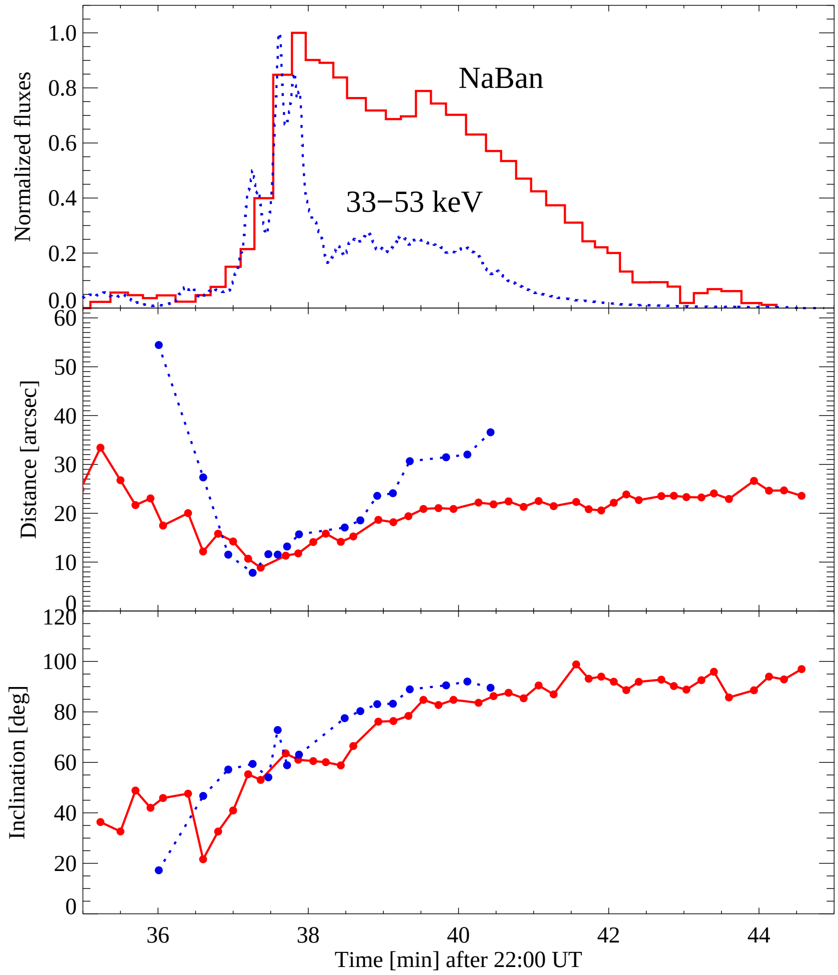

Figure 16. The time variations of the distance (middle panel) and inclination (bottom panel) of the line joining the two main emission patches (in **a** and **b** areas) as observed on NaBan deconvolved images (solid line) and M2 HXT images (dotted line) for the flare on 15 November 1991. The top panel shows NaBan and M2 HXT normalized light curves for the comparison.

be preserved for the other times during flare evolution. This is evident from Figures 9 and 16 where the separations and inclinations in WL and HXT images do not match.

The observed two main emission patches in areas **a** and **b** change their relative position during the flare evolution. This changes are illustrated in Figure 16. In the middle panel we have plotted the time variations of the distance between the patches (dashed line for the HXT M2 channel and solid line for the white light emission). In the bottom panel we present the time variations of inclination of the line connecting both patches. Similar trend of changes for the separation and inclination can be seen for both WL and HXT emissions. The strongest variability is observed during the impulsive phase. Initially the separation of the patches decreases (phase before the maximum of the impulsive phase) and increases again systematically afterwards. At the flare maximum phase the separation between WL and HXT patches is about the same, however the patches do not coincide spatially. The inclination tends to change (increase) from the very beginning of the event. The systematic lag exists between the inclination as observed in WL relative to the HXT. The WL inclination appears to lag behind respective HXT inclination by ~ 30 s.

3. Conclusions

Five white light flare events observed by *Yohkoh* have been analyzed in detail. The white light emission has been recorded using the NaBan (narrow band) filter with the transmission window centered around the CN band at 4300 Å. In order to increase the spatial resolution and remove instrument blurring, the NaBan images have been deconvolved using the ANDRIL maximum likelihood iterative algorithm.

The results of present analysis indicate that:

- Application of deconvolution algorithm (ANDRIL) leads to improvement of image quality (signal/noise ratio) and resolution in the SXT NaBan images.
- Many small details of 1 arc sec size can be identified in the deconvolved SXT NaBan images.
- Observed WL flare related emission is fine-structured and highly dynamic in character. Translation velocities may reach 100 km/s.
- WL emission patches tend to displace along structures resembling low lying arcades of loops several thousands km long.
- Time variations of WL emission are seen to be best correlated with the hard X-ray emission in the range 14-30 keV i.e. the softer portion of hard X-ray flare emission.
- There is no overall one-to-one correspondence between location of the WL emission and HXT emission and/or SXT emission. The sources do overlap sometimes which we interpret as projection effects.

– Emission in each spectral band appears to originate in a separate plasma volumes.

– At the location of hardest (53-93 keV) X-ray emission, the WL emission is usually missing or weak.

For the other flares not discussed in detail in this contribution, we also found the above conclusions applicable. In particular, the best correlation exists between time variations of WL (NaBan) emission and the 14-23 keV flux. For the flare on 24 October 1991, the WL emission correlates best with the *GOES* 0.5-4 Å flux. In the last column of Table I we indicate the X-ray band for which the best correlation has been observed with the WL emission.

We failed to accommodate observed properties of the investigated WL flares with present scenarios for the WL emission excitation mechanisms (i.e. particle precipitation, soft X-ray illumination).

It appears that the WL, SXT and HXT emissions are somewhat related, however indirectly. A higher level process(es) are envisaged to influence (in somewhat different way) activation of energy release in each of energy bands considered.

Acknowledgements

We would like to thank unknown Referee for important comments leading to improvement of the present paper. This work has been supported by the grant "*Organisation of the Magnetic Fields in the Corona*" (2.P03D.024.17) of Polish Committee for Scientific Research.

References

Ding, M.D., Fang, C., and Yun, H.S.: 1999, *Astrophys. J.* **512**, 454.

Fang, C., Yin, S.Y., Hiei, E., Ding, M.D., and Fu, Q.J.: 1995, *Solar Phys.* **158**, 387.

Hudson, H.S., Acton. L.W., Hirayama. T., and Uchida, Y.: 1992, *Publ. Astron. Soc. Japan NRO Report*, **44**, L77.

Hudson, H.S., van Driel-Gesztelyi. L., and Kosugi, T.: 1994, in *Proc. Kofu Symposium,* eds S. Enome and T. Hirayama, *NRO Report*, **360**, 397.

Lee, S.W., Yun, H.S., Hu, J., Fang, C., and Wang, J.L.: 1996, *Solar Phys.* **163**, 361.

Matthews, S.A., Brown, J.C., and van Driel-Gesztelyi, L.: 1996, in *Proc. Yohkoh Conference,* eds R.D. Bentley and J.T. Mariska, *PASP*, **111**, 304.

Matthews, S.A., Brown, J.C., and van Driel-Gesztelyi, L.: 1998, *Astron. Astrophys.* **340**, 277.

Rieger, E., Neidig, D.F., Engfer, D.W., and Strelow, D.: 1996, *Solar Phys.* **167**, 307.

Siarkowski, M., Sylwester, J., Jakimiec, J., and Tomczak, M.: 1996, *Acta Astron.* **46**, 15.

Sylwester, J., and Sylwester, B.: 1998, *Acta Astron.* **48**, 519.
Sylwester, J., and Sylwester, B.: 1999, *Acta Astron.* **49**, 189.